

Optical properties of YSAG:Yb:Er ceramics with Sc³⁺ cations in the dodecahedral and octahedral positions of the garnet crystal lattice

Vitaly A. Tarala¹, Alexander A. Kravtsov¹, Sergey V. Kuznetsov^{1,2}, Fedor F. Malyavin¹, Oleg M. Chapura¹, Ekaterina A. Brazhko¹, Lev V. Kozhitov³

¹ North Caucasian Federal University, 1 Pushkin Str., Stavropol 355017, Russian Federation

² Prokhorov General Physics Institute of the Russian Academy of Sciences, 38 Vavilov Str., Moscow 119991, Russian Federation

³ National University of Science and Technology "MISIS", 4-1 Leninsky Ave., Moscow 119049, Russian Federation

Corresponding author: Vitaly A. Tarala (vitaly-tarala@yandex.ru)

Received 19 September 2023 ♦ Accepted 27 September 2023 ♦ Published 12 October 2023

Citation: Tarala VA, Kravtsov AA, Kuznetsov SV, Malyavin FF, Chapura OM, Brazhko EA, Kozhitov LV (2023) Optical properties of YSAG:Yb:Er ceramics with Sc³⁺ cations in the dodecahedral and octahedral positions of the garnet crystal lattice. *Modern Electronic Materials* 9(3): 133–144. <https://doi.org/10.3897/j.moem.9.3.115403>

Abstract

Optical ceramics based on YSAG:Yb:Er with the compositions {Y_{1.86}Yb_{0.45}Er_{0.09}Sc_{0.6}}[Al_{1.6}Sc_{0.4}]Al₃O₁₂ and {Y_{2.26}Yb_{0.45}Er_{0.09}Sc_{0.2}}[Al_{1.0}Sc_{1.0}]Al₃O₁₂ were fabricated by vacuum sintering from pre-synthesized nanocrystalline powders. A comparative analysis of these samples with optical ceramics of the compositions {Y_{2.34}Yb_{0.45}Er_{0.09}Sc_{0.12}}[Al_{1.92}Sc_{0.08}]Al₃O₁₂ and {Y_{0.96}Yb_{0.45}Er_{0.09}Sc_{1.50}}[Al_{1.8}Sc_{0.2}]Al₃O₁₂ was carried out. The influence of scandium cations in the dodecahedral and octahedral positions of the garnet crystal lattice on the refractive index of YSAG:Yb:Er, as well as the values of absorption coefficients, integral luminescent intensities, and lifetimes of excited states of Yb³⁺ (²F_{7/2} and ²F_{5/2}) and Er³⁺ (⁴I_{15/2}, ⁴I_{13/2}, ⁴F_{9/2}, and ⁴S_{3/2}) cations was revealed in the wavelength ranges 520–700 nm and 890–1690 nm. It has been shown that by changing the concentrations of scandium cations in the dodecahedral and octahedral positions of the crystal lattice of YSAG:Yb:Er solid solutions, it is possible to purposefully change the efficiency of energy transfer from ytterbium cations to erbium cations.

Keywords

yttrium scandium aluminum garnet, solid solution, ceramics, optical properties, luminescence

1. Introduction

Materials doped with erbium (Er³⁺) cations are utilized for the creation of active media for lasers [1–6], Stokes and anti-Stokes phosphors [7–10]. The main disadvantage of Er³⁺ cations is the small absorption cross section at diode pumping wavelengths of 940 and 980 nm, which has a negative effect on the efficiency of laser radiation

generation. One of the ways to solve this problem is the sensitization of erbium with ytterbium cations, since the absorption cross section of Yb³⁺ cations at a wavelength of 980 nm is about $1.2 \cdot 10^{-20}$ cm², and for Er³⁺ about $1.7 \cdot 10^{-21}$ cm². In this regard, the actual problem is the development of solid solutions in which Yb³⁺ cations can efficiently absorb exciting radiation and transfer it to Er³⁺ ions [11–13]. The laser and luminescent characteristics of

various oxide matrices doped with Er³⁺ and Yb³⁺ cations are actively studied, among which the most attention is paid to yttrium aluminum garnets (YAG) [2, 11, 12, 14], ytterbium aluminum garnets (YbAG) [15, 16], lutetium aluminum garnets (LuAG) [6, 17] and gadolinium gallium garnets (GGG) [18].

Scandium-containing solid solutions with a garnet structure deserve special attention, since on their basis it is possible to obtain solid solutions with a disordered structure of the garnet crystal lattice, which leads to a change in the crystal field and broadening of the absorption bands of Yb³⁺ cations [12, 19–21] and Er³⁺ cations [22]. The broadening of the absorption bands of Yb³⁺ and Er³⁺ makes it possible to increase the overlap of their absorption bands and the efficiency of energy transfer processes from one cation to another.

The crystal structure of the garnet lattice is described by the formula $\{C_3\}[A_2](D_3)O_{12}(Ia-3d)$ [23], where *C*, *A*, and *D* represent dodecahedral, octahedral, and tetrahedral positions, respectively. In YSAG:Yb:Er solid solutions, yttrium (Y³⁺), erbium (Er³⁺), and ytterbium (Yb³⁺) cations occupy the *C* positions, while the *A* and *D* positions are occupied by aluminum cations (Al³⁺). Depending on the composition in the garnet crystal lattice, scandium can occupy both *C*- and *A*-positions. It was shown that scandium cations in the *C* and *A* positions do not have an equivalent effect on the energy structure of Er³⁺ cations in the YSAG:Er matrix [22]. This means that the properties of the YSAG:Yb:Er compositions with the predominant incorporation of scandium cations into the dodecahedral position of the garnet crystal lattice differ from the properties of solid solutions with the predominant inclusion of scandium in the corresponding octahedral position. It was demonstrated that in YSAG:Yb:Er solid solutions, the ratios of the integrated intensities of the Stokes luminescence bands of the Yb³⁺ (${}^2F_{5/2} \rightarrow {}^2F_{7/2}$) and Er³⁺ (${}^4I_{13/2} \rightarrow {}^4I_{15/2}$) cations, as well as the anti-Stokes luminescence bands of the cations Er³⁺ (${}^4S_{3/2} \rightarrow {}^4I_{15/2}$) and (${}^4F_{9/2} \rightarrow {}^4I_{15/2}$) depend on the concentration of scandium cations in the dodecahedral (*C*-position) of the garnet crystal lattice [24]. There are no unambiguous data on the effect of scandium cations in the octahedral (*A*-position) on the luminescence properties of YSAG:Yb:Er, as well as the dependence of the lifetimes of the excited states of Yb³⁺ and Er³⁺ cations on the predominant incorporation of Sc³⁺ cations into the *C*- or *A*-position.

The results of these studies are necessary for understanding the nature of the properties of YSAG:Yb:Er solid solutions. They also help determine the compositions with potential applications in creating lasers, Stokes phosphors, or anti-Stokes phosphors based on them.

In this regard, the aim of the study was to reveal the effect of scandium cations content in the dodecahedral and octahedral positions of the crystal lattice of solid solutions with a garnet structure on the optical and luminescent properties of YSAG:Yb:Er.

2. Materials and methods

2.1. Synthesis of YSAG:Yb:Er powders and ceramics

It is advisable to consider the YSAG:Yb:Er solid solutions formed in the system of oxide compositions Y₂O₃–Er₂O₃–Yb₂O₃–Sc₂O₃–Al₂O₃ as substitutional solid solutions in the matrix of yttrium-aluminum garnet (Y₃Al₂Al₃O₁₂). Since the ionic radii of ytterbium ($R(\text{Yb}_C^{3+}) = 0.0985$ nm) and erbium ($R(\text{Er}_C^{3+}) = 0.1004$ nm) are close to the ionic radius of yttrium ($R(\text{Y}_C^{3+}) = 0.1019$ nm), then they occupy dodecahedral positions. Aluminum cations are located in octahedral (Al_A³⁺) and tetrahedral (Al_D³⁺) positions. Scandium can be incorporated into dodecahedral (Sc_C³⁺) and octahedral (Sc_A³⁺) positions [25–26]. Previously, it was reported on the synthesis and study of the properties of scandium-containing garnets (YSAG:Yb:Er) compositions:

- Y_{2.34}Yb_{0.45}Er_{0.09}Sc_{0.2}Al_{1.92}Al₃O₁₂ (AP1),
- Y_{1.66}Yb_{0.45}Er_{0.09}Sc_{1.0}Al_{1.8}Al₃O₁₂ (AP2) and
- Y_{0.96}Yb_{0.45}Er_{0.09}Sc_{1.70}Al_{1.8}Al₃O₁₂ (AP3) [24].

In this work, the following YSAG:Yb:Er optical ceramics samples were manufactured: Y_{1.86}Yb_{0.45}Er_{0.09}Sc_{1.0}Al_{1.6}Al₃O₁₂ (CA20) and Y_{2.26}Yb_{0.45}Er_{0.09}Sc_{1.2}Al_{1.0}Al₃O₁₂ (A50), which were distinguished by increased concentrations of Sc³⁺ cations. In particular, in sample CA20, the concentration of Sc_A³⁺ = Sc_C³⁺ = 20 at.%, and in sample A50, the concentration of Sc_A³⁺ is 50 at.%, while Sc_C³⁺ content is 6.67 at.%. At the same time, in samples CA20 and A50, as well as in the samples from ref. [24], the concentrations of Yb_C³⁺ and Er_C³⁺ cations were 15 at.% and 3 at.%, respectively.

Samples of optical ceramics were fabricated through non-reactive sintering of nanocrystalline powders of yttrium-scandium-aluminum garnets doped with ytterbium and erbium cations (YSAG:Yb:Er). The precursor powders were synthesized via reverse chemical precipitation of concentrated salt solutions: AlCl₃•6H₂O (99.9%, Acros Organics, Belgium), ScCl₃•6H₂O (99.9%, Vekton, Russia), ErCl₃•6H₂O (99.9%, Vekton, Russia), YbCl₃•6H₂O (99.9%, Vekton, Russia), YCl₃•6H₂O (99.9%, Chemical Point, Germany). A concentrated ammonia solution (25%) with the addition of ammonium sulfate (0.45 mol./l) was used as a precipitant. The resulting precipitate was washed with ammonium sulfate solution (0.045 M) through centrifugation. The washed precipitate was dried at 60 °C for 20 h. Next, the powders were wet ground in a planetary mill for 30 min. in an aqueous medium using zirconium dioxide balls. At this stage, magnesium chloride was introduced into the precursor powders as a precursor of magnesium oxide (MgO), which was used as a sintering additive. The calculated concentration of MgO was fixed and amounted to 0.75 mol.%. Synthesis of YSAG:Yb:Er ceramic powders were carried out by calcination the precursor powder in air at a temperature of 1200 °C during 2 h.

Next, the ceramic powders were ground in an ethanol medium using zirconia balls in a Pulverisette 5 planetary mill for 20 min., followed by drying at 60 °C for 20 h.

In this way, nanocrystalline powders with crystallite size $\approx 60 \pm 5$ nm and specific surface area $\approx 9,2 \pm 1,1$ m²/g were obtained.

Small portions of powder were taken from each sample of YSAG : Yb : Er ceramic powders to obtain microcrystalline powders. These microcrystalline powders were used to check the phase composition of the studied oxide compositions. The samples were calcined in air at a temperature of 1600 °C using a high-temperature furnace NT 40/17 (Nabertherm GmbH). The duration of isothermal exposure was 2 h.

Ceramic powders were uniaxially pressed into the green bodies with a diameter of 15 mm and a thickness of 4 mm at a pressure of 50 MPa.

Sintering of ceramic samples was carried out in an “SShVE-1.2.5/25” vacuum furnace (LLC “VNIIE TO”). The residual pressure in the vacuum furnace chamber did not exceed $5 \cdot 10^{-5}$ Pa.

The obtaining ceramic samples were subjected to double-sided grinding and mirror polishing using a Qpol-250 machine (Germany). The final thickness of all samples was 1.00 ± 0.01 mm.

2.2. Research methods

The phase composition of YSAG : Yb : Er powders was determined by XRD-method. A diffractometer Empyrean (PANalytical, Netherlands) with $\text{CuK}\alpha$ radiation ($\lambda = 0.15418$ nm, 2θ range 10–90°, with a step of 0.01°, scanning speed of 0.7°/min.) were used for XRD-investigations. Data evaluation and phase identification were performed in the HighScore Plus with the ICDD PDF-2 database.

The optical transmission spectra in the ranges of 100–200 nm and 1250–2500 nm were measured by using SF-56 and FSM-1211 (OKB Spekt, Russia) spectrophotometers, respectively.

Measurements aimed at determining the refractive index of YSAG : Yb : Er optical ceramic samples were carried out by using a SE-800 spectroscopic UV-VIS ellipsometer (SENTECH Instruments GmbH, Germany). The results of ellipsometry were analyzed using SpectraRay/3 software.

The luminescence spectra of the ceramic samples were measured by using a SFL-MDR spectrofluorimeter (OKB Spectr, Russia). The R928 photomultiplier tube (Hamamatsu Photonics, Japan) and G12180 semiconductor detector (Hamamatsu Photonics, Japan) were used for measuring at 300–900 nm and 900–1800 nm spectral ranges respectively.

Luminescence kinetics at wavelengths of 561 nm, 679 nm and 1029 nm was studied using SFL-MDR spectrofluorimeter (OKB Spectr, Russia). An SFL-MDR-2 spectrofluorimeter (OKB-Spekt, Russia) was used to study the luminescence kinetics in the region of 1535 nm.

3. Results and discussion

3.1. XRD-analysis results

Studies of the phase composition of microcrystalline powders CA20 and A50 showed that they are solid solutions with a garnet structure (Fig. 1). No impurity phases were detected. This indicates that all cations are distributed over positions of the garnet crystal lattice.

The samples differed in the values of the crystal lattice parameters (a_G) (Table 1). The highest a_G value was recorded for sample A50, whose crystal lattice parameter was 0.01400 nm greater than that of AP1 and 0.05705 nm greater than that of sample AP3. High values of a_G can be explained by the fact that the ionic radius of the Sc_A^{3+} cation ($R(\text{Sc}_A^{3+}) = 0.0745$ nm) is greater than the ionic radius of the Al_A^{3+} cation ($R(\text{Al}_A^{3+}) = 0.0535$ nm) [27]. Therefore, according to Vegard’s law [28], an increase in a_G is due to

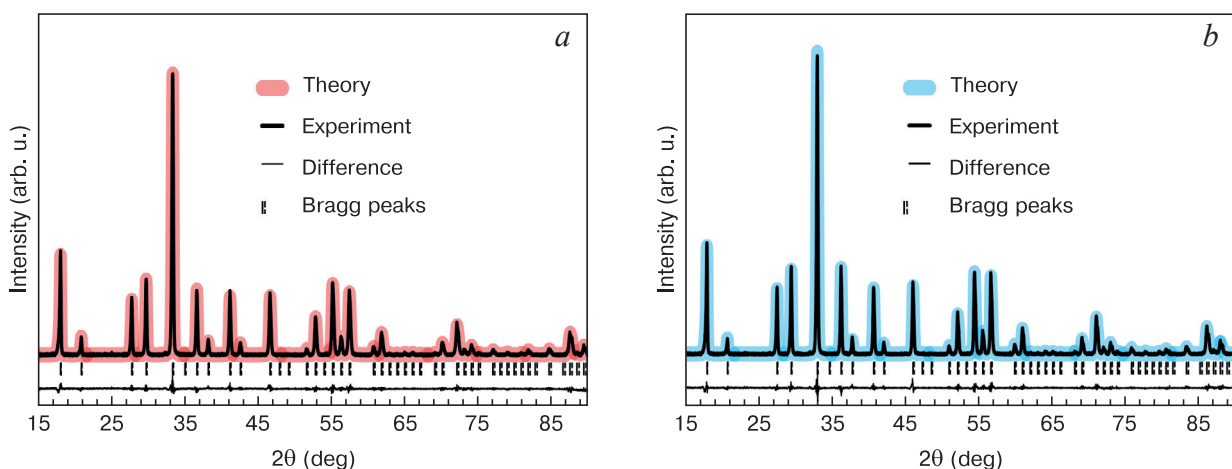


Figure 1. X-ray diffraction patterns for YSAG : Yb : Er: (a) CA20; (b) A50

Table 1. Results of analysis of the phase composition of oxide compositions

Sample	Garnet phase composition	Sc _C ³⁺ (at.%)	Sc _A ³⁺ (at.%)	a _G (nm)	a _{SV} (nm)	Ref.
AP1	{Y _{2.34} Yb _{0.45} Er _{0.09} Sc _{0.12} }[Al _{1.92} Sc _{0.08}]Al ₃ O ₁₂	4	4	1.20044	1.2002	[24]
AP3	{Y _{0.96} Yb _{0.45} Er _{0.09} Sc _{1.50} }[Al _{1.8} Sc _{0.2}]Al ₃ O ₁₂	50	10	1.18735	1.1873	[24]
CA20	{Y _{1.86} Yb _{0.45} Er _{0.09} Sc _{0.6} }[Al _{1.6} Sc _{0.4}]Al ₃ O ₁₂	20	20	1.20045	1.2003	This work
A50	{Y _{2.26} Yb _{0.45} Er _{0.09} Sc _{0.2} }[Al _{1.0} Sc _{1.0}]Al ₃ O ₁₂	6.67	50	1.21444	1.2144	This work

a decrease in the proportion of Al_A³⁺ and an increase in the proportion of Sc_A³⁺. The comparable a_G values of samples AP1 [24] and C20 indicate mutual compensation of the effects of stretching and compression of the crystal lattice associated with the Sc_A³⁺ and Sc_C³⁺ cations, respectively.

Theoretical estimation of the crystal lattice parameters of scandium-containing garnets (a_{SV}) was made using the equation [25]:

$$a_{SV} = (a_S + a_V)/2,$$

$$a_S = 7.02954 + 3.31277r_C + 2.49398r_A + 3.34124r_D - 0.87758r_{C^*A} - 1.38777r_{C^*D};$$

$$a_V = 10.092217 + 0.841118r_C + 0.734598r_A - 2.507813r_D + 3.133970r_{C^*D} + 1.946901r_{A^*D};$$

$$r_C = [Y_C^{3+}]R(Y_C^{3+}) + [Yb_C^{3+}]R(Yb_C^{3+}) + [Er_C^{3+}]R(Er_C^{3+}) + [Sc_C^{3+}]R(Sc_C^{3+});$$

$$r_A = [Al_A^{3+}]R(Al_A^{3+}) + [Sc_A^{3+}]R(Sc_A^{3+});$$

$$r_D = [Al_D^{3+}]R(Al_D^{3+});$$

$$[Y_C^{3+}] + [Yb_C^{3+}] + [Er_C^{3+}] + [Sc_C^{3+}] = 1;$$

$$[Al_A^{3+}] + [Sc_A^{3+}] = 1;$$

$$[Al_D^{3+}] = 1.$$

where a_S is the crystal lattice parameter in Strook's empirical formula [29]; a_V is the crystal lattice parameter in Vorobiev's empirical formula [30]; [Y_C³⁺], [Yb_C³⁺], [Er_C³⁺], [Sc_C³⁺], [Al_A³⁺], [Sc_A³⁺], [Al_D³⁺] – concentrations of cations in the corresponding positions of the YSAG:Yb:Er crystal lattice; R(Y_C³⁺), R(Yb_C³⁺), R(Er_C³⁺), R(Sc_C³⁺), R(Al_A³⁺), R(Sc_A³⁺), R(Al_D³⁺) – Shannon ionic radii of cations [27]. Good agreement between the values of a_{SV} and a_G indicates that the planned and actual compositions of the garnet phases coincide. Modeling X-ray diffraction patterns using the Rietveld method allowed for an additional assessment of the concentrations of scandium cations in the dodecahedral and octahedral positions of the garnet crystal lattice. The initial coordinates of oxygen for the space group *Ia3d* (number 230) were taken from [31]. In the simulation, it was assumed that the 24d positions are occupied by Al_D³⁺ cations, and in positions 24c – cations Y_C³⁺, Yb_C³⁺, Er_C³⁺ and Sc_C³⁺. In position 16a,

cations Al_A³⁺ and Sc_A³⁺ are present, and in positions 96 h, oxygen is located. Fig. 1 shows that the results of modeling and experimental studies of microcrystalline powders are in good agreement, which allows us to assert that the planned and actual compositions of the samples coincide.

3.2. Characterization of the optical ceramics samples

Samples of optical ceramics were obtained by sintering compacts of nanocrystalline powders in a vacuum furnace. The optimum vacuum sintering temperatures were found to be 1850 °C and 1775 °C for A50 and CA20, respectively. The values of the optimal sintering temperatures are in good agreement with the results of previous studies of YSAG:Yb [32] and YSAG:Er [26] solid solutions with comparable concentrations of Sc³⁺ cations for A and C sites. Photographs of optical ceramic samples after polishing are shown in Fig. 2 a. The samples were characterized by high transmittance in the visible region of the spectrum (Fig. 2 b), which allows them to be classified as optically transparent.

Analysis of the transmission spectra of YSAG:Yb:Er samples showed that they are similar to the spectra of YAG:Yb:Er [12] and YSAG:Yb:Er [24], since they contain absorption bands associated with the presence of Er³⁺ and Yb³⁺ cations.

3.3. Refractive index dispersion

Table 2 shows the parameters of the Sellmeyer model [33, 34] for the manufactured YSAG:Yb:Er samples. This model describes the refractive index dispersion (*n*(λ)) for the bulk layer:

$$n(\lambda) = \left(\varepsilon(\infty) + \frac{A\lambda^2}{\lambda^2 - B^2} - C\lambda^2 \right)^{1/2},$$

where *n*(λ) is the refractive index at wavelength λ, ε(∞) is the high-frequency dielectric constant of the material, A, B and C are the parameters of the Sellmeyer model. The corresponding refractive index dispersions of the samples are presented in Fig. 3.

According to the data presented in Table 2, the refractive index values (*n*) at a wavelength of 632.8 nm for the samples A50 (Sc_A³⁺ = 50 at.%, Sc_C³⁺ = 6.67 at.%) and CA20 (Sc_A³⁺ = Sc_C³⁺ = 20 at.%) are comparable in magnitude with the *n* values of the sample AP3 (Sc_A³⁺ = 10 at.%, Sc_C³⁺ = 50 at.%) within the limits of error [24]. Note that

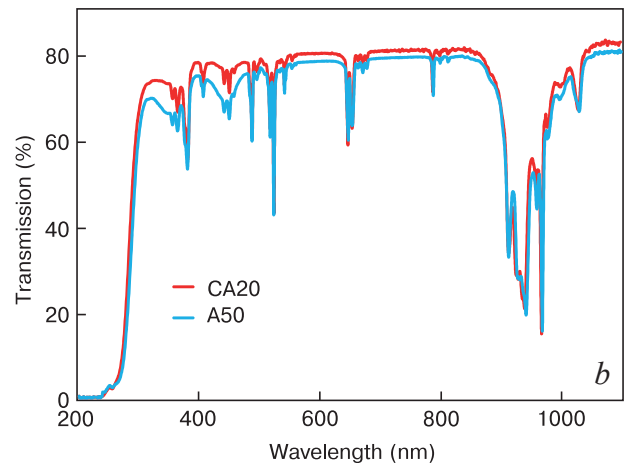
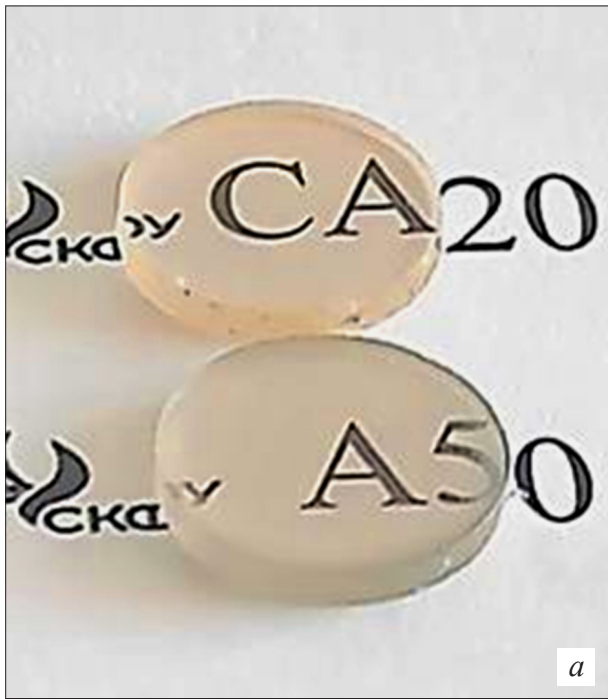


Figure 2. Photographs of YSAG : Yb : Er ceramic samples (a) and light transmission spectra (b)

Table 2. Calculation parameters of the ellipsometric model

Sample	$n(632.8)$	ϵ_∞	A	B	C	Roughness (nm)	MSE	Ref.
AP1	1.827±0.005	1.880	1.402	0.130	0.014679	4.2	0.755	[24]
AP3	1.859±0.005	2.050	1.302	0.137	0.012103	5.7	0.869	[24]
CA20	1.854±0.005	1.876	1.491	0.139	0.01310	8.75	0.67	This work
A50	1.859±0.005	1.907	1.482	0.136	0.01325	4.37	0.93	This work

for single crystals, the following n values were registered: $Y_3Al_5O_{12}$ $n = 1.829$ [35], $Y_3Sc_1Al_4O_{12}$ – 1.850 [36], and $Y_3Sc_2Al_3O_{12}$ – 1.873 [34].

It should be noted that the established "n" values in YSAG : Yb : Er samples with different concentrations of Sc_A^{3+} and Sc_C^{3+} cations are in good agreement with the results of previously conducted studies of YSAG : Cr solid solutions [37], which had comparable concentrations of

scandium in the dodecahedral and octahedral positions of the crystal lattice. This circumstance allows us to conclude that an increase in the concentration of scandium at any position of the crystal lattice leads to an increase in the refractive index of a solid solution with a garnet structure.

3.4. Absorption spectra

Earlier, in [24], it was noted that the influence of scandium cations in the dodecahedral and octahedral positions of YSAG : Yb : Er on the properties of Yb^{3+} and Er^{3+} cations can be neglected at concentrations of cations Sc_C^{3+} and Sc_A^{3+} up to 4 at.%. In particular, it was shown that the absorption spectrum of Yb^{3+} cations in the YSAG : Yb : Er sample (composition AP1) and YAG : Yb [38, 39] and YAG : Yb : Er [12] ceramics is similar. As a rule, the spectrum of Yb^{3+} cations contains several Stark absorption bands (SB). At the same time, the bands $SB(v_0 \rightarrow v_5)$ and $SB(v_0 \rightarrow v_4)$ deserve special attention, since their absorption maxima are located in the region of laser pumping wavelengths of commercially produced InGaAs LEDs.

Figure 4 shows the absorption spectra of Yb^{3+} cations in samples CA20 and A50. For comparison, the spectrum of sample AP1 [24] is shown, for which the absorption

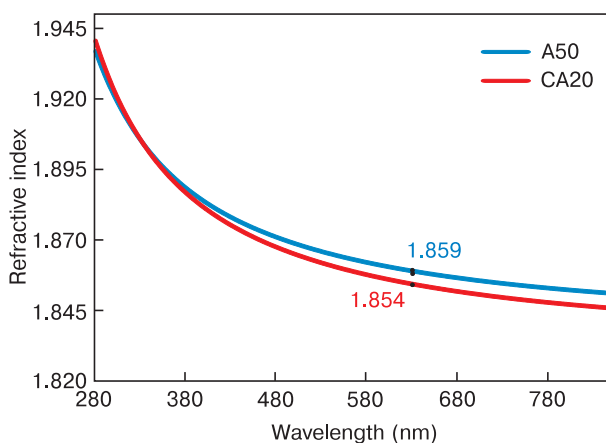


Figure 3. Spectral dependences of the refractive index of samples A50 and CA20

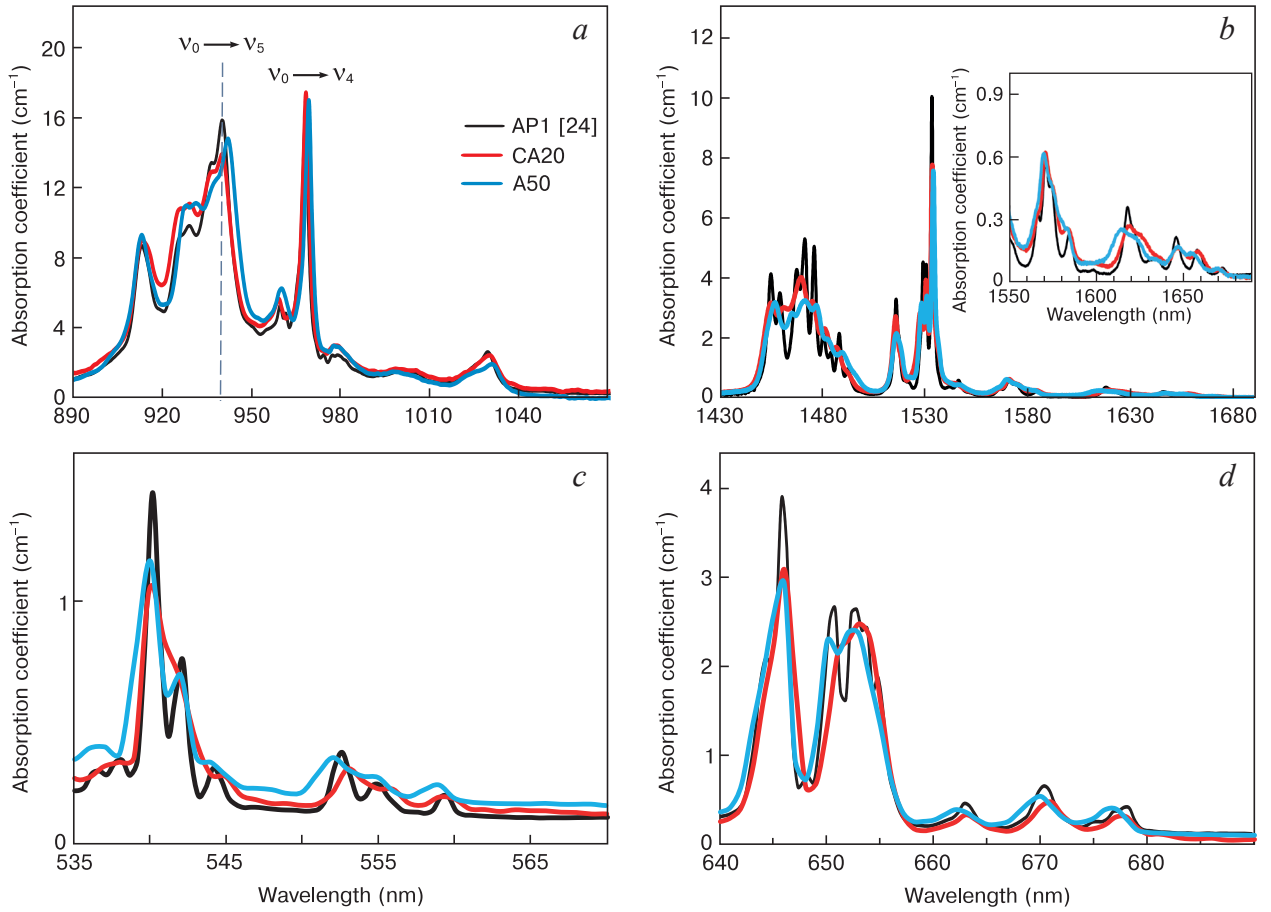


Figure 4. Absorption spectra of the YSAG:Yb:Er samples: (a) Yb_C^{3+} (${}^2F_{7/2} \rightarrow {}^2F_{5/2}$ term, 890–1065 nm), (b) Er_C^{3+} (${}^4I_{15/2} \rightarrow {}^4I_{13/2}$, 1430–1690 nm), (c) Er_C^{3+} (${}^4I_{15/2} \rightarrow {}^4S_{3/2}$, 535–565 nm), (d) Er_C^{3+} (${}^4I_{15/2} \rightarrow {}^4F_{9/2}$, 640–690 nm)

coefficients (AC) are approximately 16 cm^{-1} for the absorption bands $\text{SB}(v_0 \rightarrow v_5)$ and $\text{SB}(v_0 \rightarrow v_4)$ at wavelengths 939 nm and 968 nm, respectively.

In sample A50, with the concentration of Sc_A^{3+} of 50 at.%, the $\text{SB}(v_0 \rightarrow v_5)$ band is shifted by 1.0–1.5 nm to the region of longer wavelengths, while the ratio of absorption coefficients $\text{AC}(v_0 \rightarrow v_4)/\text{AC}(v_0 \rightarrow v_5)$ increased to 1.15.

Despite the fact that in sample CA20 the concentrations of Sc_A^{3+} and Sc_C^{3+} are five times higher than in sample AP1, the positions of the maxima of their $\text{SB}(v_0 \rightarrow v_4)$ bands and $\text{SB}(v_0 \rightarrow v_5)$ bands coincided. However, for sample CA20, the ratio of absorption coefficients turned out to be higher than $\text{AC}(v_0 \rightarrow v_4)/\text{AC}(v_0 \rightarrow v_5)$ at approximately 1.2.

Since the Sc_C^{3+} and Sc_A^{3+} cations do not directly participate in light absorption processes, the detected changes in the spectra of the Yb_C^{3+} cations are probably associated with disordering of the crystal field caused by the partial replacement of yttrium and aluminum with scandium cations. As shown in [24], if the concentration of Sc_C^{3+} increases in the immediate environment of the Yb_C^{3+} cation, then the maximum $\text{SB}(v_0 \rightarrow v_5)$ shifts to the blue region of the spectrum, while the ratio $\text{AC}(v_0 \rightarrow v_4)/\text{AC}(v_0 \rightarrow v_5)$ increases. In this study, it was found that if the concentration of Sc_A^{3+} increases in the immediate environment of

the Yb_C^{3+} cation, then the maximum $\text{SB}(v_0 \rightarrow v_5)$ shifts to the red region of the spectrum. Thus, it can be argued that Yb_C^{3+} cations, in the immediate environment of which Sc_C^{3+} cations or Sc_A^{3+} cations dominate, are not equivalent.

Figure 4 b shows a section of the absorption spectrum of Er_C^{3+} cations for the ${}^4I_{15/2} \rightarrow {}^4I_{13/2}$ transition. Note that the ${}^4I_{15/2}$ term consists of 8 Stark energy levels, and the ${}^4I_{13/2}$ term consists of 7 levels [40]. It was found that in samples A50 and CA20, the number of distinguishable peaks is smaller compared to sample AP1. This is most clearly manifested in the wavelength range from 1440 to 1500 nm (Fig. 4 b). In our opinion, the decrease in discernible peaks clearly indicates a broadening of the absorption bands due to disordering of the crystal field. The main reason is an increase in the concentration of Sc_C^{3+} and Sc_A^{3+} .

It is important to note that the Stark band has the highest absorption coefficient at a wavelength of 1532 nm. This band is associated with the transition of an electron from the lower Stark level of the ${}^4I_{15/2}$ term to the lower Stark level of the ${}^4I_{13/2}$ term. No significant changes in the position of the maximum of this band depending on the composition of the YSAG:Yb:Er samples were detected.

Relative to sample AP1, sample A50 has a group of Stark absorption bands in the long-wavelength part of the

spectrum (1550–1680 nm) shifted to shorter wavelengths (inset in Fig. 4 b). In sample CA20, the shift of the bands is less pronounced. The shift of the absorption bands indicates that the Sc_C^{3+} and Sc_A^{3+} cations have an unequal effect on the properties of the Er_C^{3+} cation. If we take into account that the shift of the absorption bands in the CA20 sample relative to AP1 is minimal, we can conclude that the Sc_C^{3+} and Sc_A^{3+} cations can compensate for each other's influence.

The broadening of the Stark absorption bands associated with Er_C^{3+} cations was also recorded in the wavelength ranges of 535–570 nm (Fig. 4 c) and 640–690 nm (Fig. 4 d). Analysis of the absorption spectra made it possible to establish that an increase in the concentration of Sc_A^{3+} leads to a blue shift of the majority of absorption bands associated with the $^4I_{15/2} \rightarrow ^4S_{3/2}$ and $^4I_{15/2} \rightarrow ^4F_{9/2}$ multiplets. At the same time, as shown in [24], an increase in the concentration of Sc_C^{3+} causes the opposite effect, which manifests itself in a shift of absorption bands towards longer wavelengths.

Thus, based on the analysis of the absorption spectra, we note that the energy structure of the $^2F_{7/2}$ и $^2F_{5/2}$ (Er_C^{3+}) multiplets and the $^4I_{15/2}$, $^4I_{13/2}$, $^4F_{9/2}$ и $^4S_{13/2}$ (Er_C^{3+}) multiplets changes nonequivalently with increasing concentration of Sc_C^{3+} or Sc_A^{3+} . Consequently, the Sc_C^{3+} and Sc_A^{3+} cations have different effects on the crystal field of a solid solution with a garnet structure.

3.5. Luminescent properties

The energy structures of Yb^{3+} and Er^{3+} cations in $\text{YAG}:\text{Yb}:\text{Er}$ solid solutions demonstrates two Stokes luminescence processes (Fig. 5) [41, 42]. The first process (*H*-process) describes the electron transitions, in which the Yb_C^{3+} cations absorb photons with a wavelength of ≈ 940 nm, and transit from ground state $^2F_{7/2}$ to the excited $^2F_{5/2}$ corresponding to Stark level v_5 . After a non-radiative transition to the Stark level v_4 , a series of transitions $v_4 \rightarrow v_3$, $v_4 \rightarrow v_2$ and $v_4 \rightarrow v_0$ follow, accompanied by the

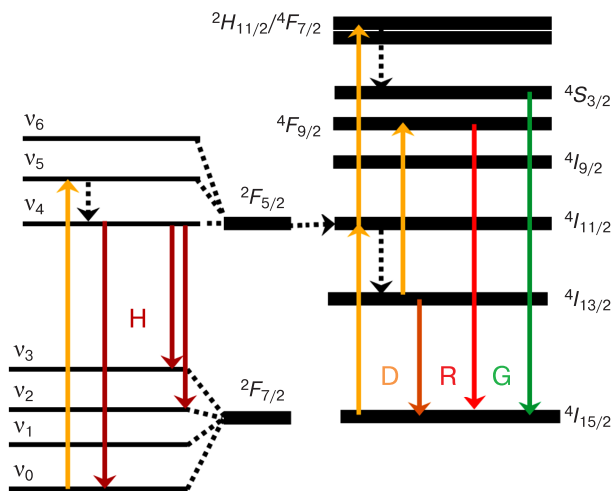


Figure 5. Scheme of the energy diagram of Yb^{3+} and Er^{3+} cations in $\text{YSAG}:\text{Yb}:\text{Er}$ [12, 41, 42]

emission of photons with wavelengths of ≈ 1050 , ≈ 1030 and ≈ 970 nm, respectively.

In the second Stokes process (*D*-process), the Yb_C^{3+} cations act as donors while the Er_C^{3+} cations act as acceptors. The transitions $^2F_{5/2} \rightarrow ^2F_{7/2}$ and $^4I_{15/2} \rightarrow ^4I_{11/2}$ have comparable values of energy, so some Yb_C^{3+} cations can transfer energy to Er_C^{3+} cations. In turn, the Er_C^{3+} ($^4I_{11/2}$) cations can give up part of their energy and pass into the $^4I_{13/2}$ excited state and then, through the $^4I_{13/2} \rightarrow ^4I_{15/2}$ transition emit photon in the wavelength range from 1450 up to 1670 nm.

According to the diagram in Fig. 5, the upconversion *G*-process of the Er_C^{3+} cation is described by the absorption of two photons by the excited state $^4I_{11/2}$, followed by its transition into the state $^4F_{7/2}$. In the next stage, non-radiative transitions occur from $^4F_{7/2}$ to $^2H_{11/2}/^4S_{3/2}$ followed by the emission of photons in the wavelength range of 540–565 nm via $^2H_{11/2}/^4S_{3/2} \rightarrow ^4I_{15/2}$ transitions.

The upconversion *R*-process is realized by energy transfer through a complicated route: $^2F_{7/2} \rightarrow ^2F_{5/2}$ (Yb) $\rightarrow ^4I_{11/2}$ (Er) $\rightarrow ^4I_{13/2}$ (Er) $\rightarrow ^4F_{9/2}$ (Er), which finalized by the luminescent transition to $^4I_{15/2}$ (Er) in the wavelength range of 645–685 nm. Since the introduction of the Sc_C^{3+} and Sc_A^{3+} cations affects the energy structure of the Yb_C^{3+} and Er_C^{3+} cations, then one should expect changes in the processes of conversion of radiation associated with the luminescence of erbium and ytterbium cations.

3.5.1. Stokes YSAG : Yb : Er luminescence

Figure 6 shows the Stokes luminescence spectra of Yb_C^{3+} cations as recorded upon excitation by laser radiation with a wavelength of approximately 940 nm. Stark luminescence bands associated with the *H*- and *D*-processes were detected in the wavelength ranges of 960–1080 nm and 1440–1690 nm, respectively. To compare the influence of Sc_C^{3+} and Sc_A^{3+} cations on the luminescent properties of $\text{YSAG}:\text{Yb}:\text{Er}$, the ratios of integral luminescence intensities ($\delta_{H/D}$) for these two processes were examined:

$$\delta_{H/D} = \frac{I_{S_H}}{I_{S_D}} = \frac{\int_{\lambda_{950}}^{\lambda_{1080}} I_H(\lambda) d\lambda}{\int_{\lambda_{1440}}^{\lambda_{1685}} I_D(\lambda) d\lambda},$$

where λ_{950} , λ_{1080} and λ_{1440} , λ_{1680} are the wavelengths of the beginning and end of the luminescence spectrum section; I_{S_H} , I_{S_D} are the integral luminescence intensities.

Analysis of the luminescence spectra reveals that the ratio of the integrated luminescence intensities for sample A50 is approximately 0.332, which is clearly greater than for sample AP1 ($\delta_{H/D} \approx 0.211$) [24]. Taking into account the cationic compositions of these samples, it can be assumed that an increase in the concentration of Sc_A^{3+} makes the *H*-process of Stokes luminescence more preferable compared to the *D*-process. At the same time, according to the data from [24], in the case of an increase in the concentration of Sc_C^{3+} , the role of the *D*-process increases. With a simultaneous increase in the concentration of cations Sc_C^{3+} and Sc_A^{3+} , their influence is mutually

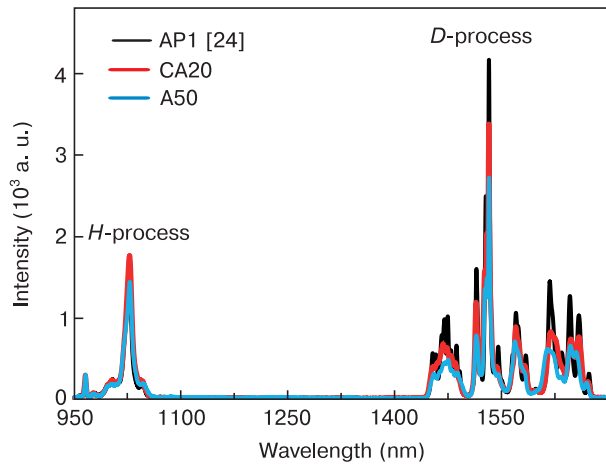


Figure 6. Luminescence spectra of the YSAG:Yb:Er samples

compensated. Therefore, the CA20 sample has a value of $\delta_{H/D}$ (≈ 0.294) greater than that of the sample AP1 but less than sample A50.

Figure 7 *a* shows the luminescence spectra of the Yb_C³⁺ cation. The broadened luminescence bands SB($v_4 \rightarrow v_2$) and SB($v_4 \rightarrow v_3$) in sample CA20 distinguish it from sample AP1 (Fig. 7 *a*). At the same time, no significant shifts of the Stark luminescence bands were detected: maximum SB($v_4 \rightarrow v_2$) ≈ 1029 nm, maximum SB($v_4 \rightarrow v_3$) ≈ 1049 nm. In our opinion, this effect may be a consequence of disordering of the crystal field due to a simultaneous increase in the concentration of Sc_C³⁺ and Sc_A³⁺ from 4 at.% to 20 at.%.

When the concentration of Sc_A³⁺ increases to 50 at.% (sample A50), there is a red shift of the SB($v_4 \rightarrow v_2$) by approximately 0.5 nm and SB($v_4 \rightarrow v_3$) by approximately 3–4 nm. It has been reported in [24] that an increase in the concentration of Sc_C³⁺ to 50 at.% leads to a red shift of the SB($v_4 \rightarrow v_2$) band by approximately 1 nm, and the SB($v_4 \rightarrow v_3$) shifts into the blue region by approximately 5–6 nm. These data show that Sc_C³⁺ and Sc_A³⁺ cations have an unequal effect on the energy structure of the Yb_C³⁺ cation.

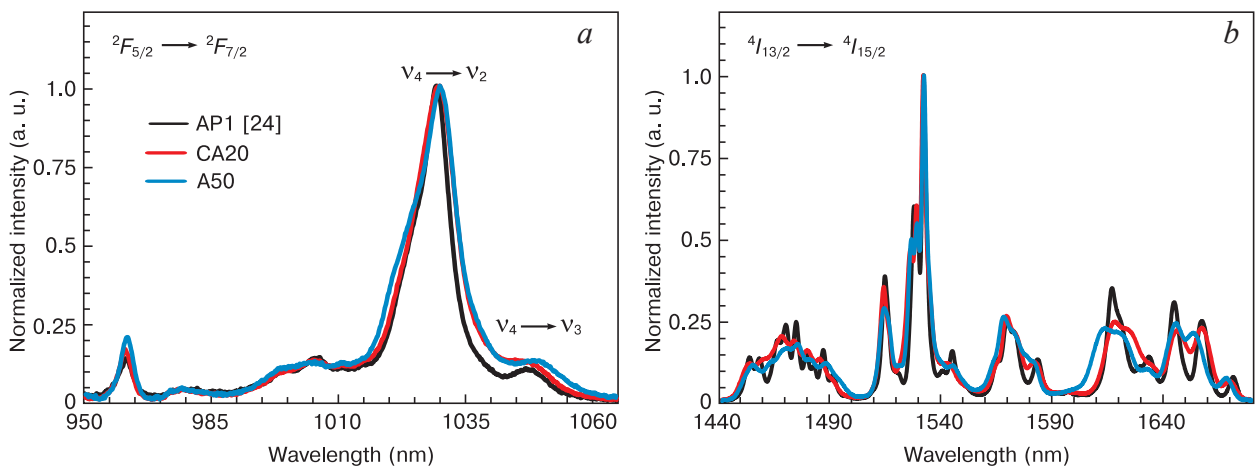


Figure 7. Normalized luminescence spectra of the Yb_C³⁺ (*a*) and Er_C³⁺ (*b*) cations in YSAG:Yb:Er samples

Fig. 7 *b* shows the normalized luminescence spectra of the Er_C³⁺ cation. Analysis of the luminescence spectra of sample A50 reveals a blue shift of the bands and broadening relative to sample AP1. This effect is presumably due to the higher concentration of Sc_A³⁺ cations compared to Sc_C³⁺ cations. This assumption is confirmed by the fact that the positions of the maxima of the luminescence bands for samples CA20 and AP1 practically coincide. It is important to note that, according to [24], an increase in the concentration of Sc_C³⁺ leads to a red shift of these bands. Therefore, we can conclude that scandium cations in different positions of the crystal lattice have an unequal effect on the energy structure and luminescent properties of the Er_C³⁺ cation.

It is important to note that the luminescence kinetics for YSAG:Yb:Er samples with different concentrations of Sc_C³⁺ and Sc_A³⁺ have not been previously considered. Therefore, to better understand the effect of scandium on the properties of YSAG:Yb:Er, in addition to the CA20 and A50 samples synthesized in this work, samples AP1 and AP3 were studied. The composition of these samples is described in Table 1, and the preparation conditions and optical properties can be found in [24]. Analysis of the luminescence kinetics (Fig. 8 *a*) revealed that in the AP3 sample, the Yb_C³⁺ cations had the shortest effective lifetime (τ) of the excited states ²F_{5/2}, while in the A50 sample, it is the longest. Moreover, the τ in sample A50 was approximately 48% greater than in sample AP3, indicating a significant influence of the position of scandium cations in the garnet crystal lattice on the properties of Yb_C³⁺ cations.

Meanwhile, the luminescence decay kinetics of samples AP1 and CA20 practically coincided with each other, probably due to the mutual compensation of the effects of the Sc_C³⁺ and Sc_A³⁺ cations. The effects of scandium cations on the decay kinetics of Stokes luminescence of Er_C³⁺ cations were less dramatic. The differences in the " τ " values indicated that the introduction of scandium cations into the dodecahedral position leads to a slight decrease in the lifetime of the excited states ⁴I_{13/2}. At the same time,

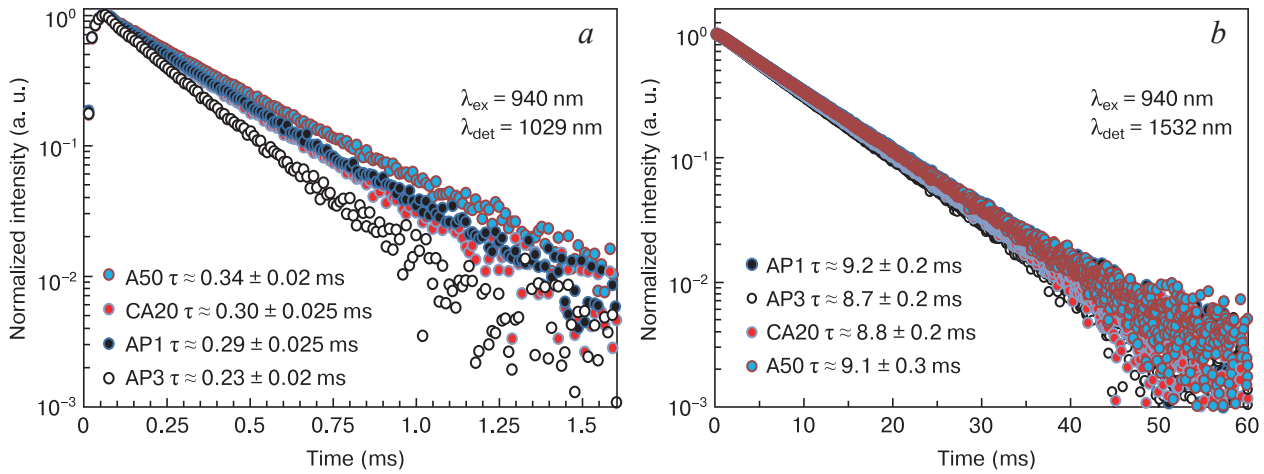


Figure 8. Luminescence decay kinetics of Yb_C^{3+} cations (a) and Er_C^{3+} cations (b)

it was found that the lifetime of the excited state $^4I_{13/2}$ of the Er_C^{3+} cation in $\text{YSAG}:\text{Yb}:\text{Er}$ (8.7–9.2 ms) is slightly higher than in $\text{YAG}:\text{Yb}:\text{Er}$ (7.0–8.5 ms) [10, 41].

Taking into account that the lifetime of the excited state is proportional to the probability of emission of light quanta, it was assumed that the probability of transitions $^2F_{5/2} \rightarrow ^2F_{7/2}$ decreases with an increasing concentration of cations Sc_A^{3+} . In this case, the probability of non-radiative energy transfer from Yb_C^{3+} cations to Er_C^{3+} cations increases. Moreover, since the value of δ_{HD} decreases, it can be argued that the transfer efficiency of energy from Yb_C^{3+} cations to Er_C^{3+} cations has also increased.

The lifetime values of the excited state $^2F_{5/2}$ of the Yb_C^{3+} cations in the AP1 sample were in good agreement with the "τ" values for $\text{YAG}:\text{Yb}(15 \text{ at.}\%):\text{Er}(1 \text{ at.}\%)$ solid solutions [41], which indicates the reliability of the obtained values. Thus, an increase in the concentration of Sc_A^{3+} was found to increase the probability of transitions $^2F_{5/2} \rightarrow ^2F_{7/2}$ while decreasing the probability of energy transfer from Yb_C^{3+} cations to Er_C^{3+} cations. Since the probability of the transition $^4I_{13/2} \rightarrow ^4I_{15/2}$ weakly depends on the concentration of scandium, the decrease in the values of δ_{HD} detected in the series of samples

$\text{A50} \rightarrow \text{AP1}(\text{CA20}) \rightarrow \text{AP3}$ indicates an increase in the efficiency of energy transfer with a decrease in the concentration of Sc_A^{3+} .

3.5.2. Anti-Stokes $\text{YSAG}:\text{Yb}:\text{Er}$ luminescence

Figure 9 shows the anti-Stokes luminescence spectra recorded upon laser radiation excitation at a wavelength of 940 nm. It is evident that regardless of the $\text{YSAG}:\text{Yb}:\text{Er}$ composition, the intensity of the luminescence bands in the green region of the spectrum is significantly lower than in the red region. The ratio of integral intensities $\delta_{G/R}$ was calculated using the expression:

$$\delta_{G/R} = \frac{I_{SG}}{I_{SR}} = \frac{\int_{\lambda_{520}}^{\lambda_{570}} I_G(\lambda) d\lambda}{\int_{\lambda_{640}}^{\lambda_{685}} I_R(\lambda) d\lambda},$$

where λ_{520} , λ_{570} and λ_{640} , λ_{680} is wavelengths of the beginning and end of the luminescence spectrum section; I_{SG} , I_{SR} is integral luminescence intensities

It was found that for sample CA20 – $\delta_{G/R} \approx 0.093$, and for A50 – $\delta_{G/R} \approx 0.12$. As shown in [24], for sample AP1 – $\delta_{G/R} \approx 0.109$, and for AP3 – $\delta_{G/R} \approx 0.088$. In this case, an increase in the values of $\delta_{G/R}$ indicates that with increasing concentration Sc_A^{3+} the probabilities of the G-process decrease noticeably than the probabilities of the R-process.

Figure 10 depicts the luminescence decay kinetics observed at approximately 561 nm and 679 nm wavelengths. To investigate the luminescence kinetics, we conducted studies on the ($^4S_{3/2} \rightarrow ^4I_{15/2}$) and ($^4F_{9/2} \rightarrow ^4I_{15/2}$) bands, utilizing light excitation at approximately 357 nm and 478 nm wavelengths, respectively.

Analysis of the obtained dependencies indicates that the lifetime of the excited state $^4S_{3/2}$ of the Er_C^{3+} cation is about $12 \pm 4 \mu\text{s}$, which is in good agreement with the data for $\text{YAG}:\text{Er}$ [44]. For the term $^4F_{9/2}$ $\tau \approx 20 \pm 5 \mu\text{s}$. As can be seen in Fig. 10, within the error, the lifetimes of the excited states of the $^4S_{3/2}$ and $^4F_{9/2}$ terms of the Er_C^{3+} cations are practically independent of the concentration of the Sc_C^{3+} and Sc_A^{3+} cations. This circumstance indicates

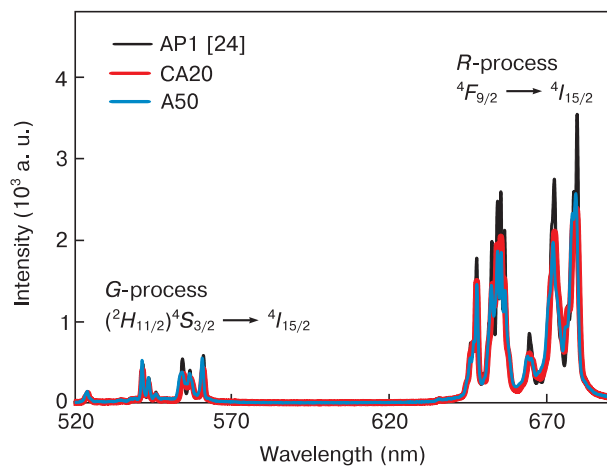


Figure 9. Anti-Stokes luminescence spectra of the $\text{YSAG}:\text{Yb}:\text{Er}$ samples

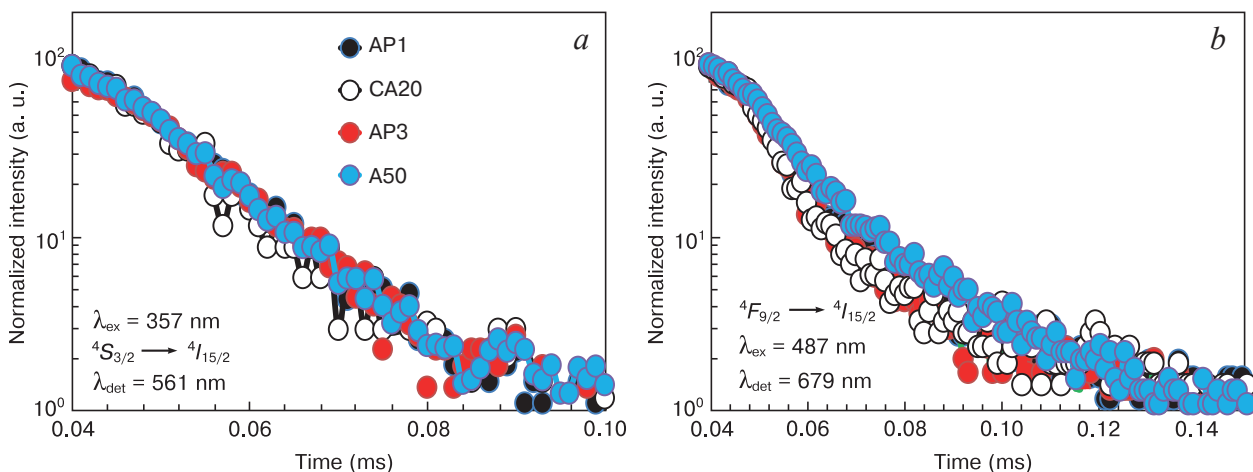


Figure 10. Luminescence decay kinetics in the green (a) and red (b) spectral range

that the excited states of Er³⁺ cations are less sensitive to the presence of scandium cations than Yb³⁺ cations. Thus, analysis of luminescence in the visible region of the spectrum confirmed the assumption that scandium cations in dodecahedral and octahedral positions have non-equivalent effects on the properties of rare earth cations. Consequently, by changing both the total concentration of scandium in the crystal lattice and the Sc_C³⁺/Sc_A³⁺ ratio, it is possible to purposefully change the properties of YSAG:Yb:Er solid solutions.

4. Conclusion

In this study, YSAG:Yb:Er optical ceramics were fabricated by non-reactive vacuum sintering of nanocrystalline powders. These ceramics contained different concentrations of scandium cations in the octahedral Sc_A³⁺ and dodecahedral Sc_C³⁺ positions of the garnet crystal lattice. The linear transmittances of mirror-polished YSAG:Yb:Er samples exceeded 80% in the region of 1.1 μm. It was found that in YSAG:Yb:Er solid solutions, an increase in the concentration of scandium cations in the octahedral position from 4 at.% up to 50 at.% led to an increase in the refractive index from 1.827 ± 0.005 to 1.859 ± 0.005.

By analyzing the absorption and luminescence spectra, it is shown that the Sc_C³⁺ and Sc_A³⁺ cations

have a non-equivalent effect on the crystal field of the YSAG:Yb:Er solid solution. It has been established that with an increase in the concentration of Sc_C³⁺ to 50 at.%, the lifetime of the excited states of the Yb_C³⁺ cation corresponding to the lower level of the ²F_{5/2} term decreases to approximately 0.23 ± 0.02 ms, and with increasing the concentration Sc_A³⁺ to 50 at.%, on the contrary, it increases to approximately 0.34 ± 0.02 ms.

It has been shown that the lifetime of excited states of the Er_C³⁺ cation weakly depends on the concentration of scandium cations and is approximately 9.0 ± 0.4 μs for the lower level of the ⁴I_{13/2} term, 12 ± 4 μs for the lower level of the ⁴S_{3/2} term, and 20 ± 5 μs for the lower level of the ⁴F_{9/2} term.

The possibility of purposefully changing the efficiency of energy transfer from Yb_C³⁺ cations to Er_C³⁺ cations and further Stokes and anti-Stokes conversion of light by measuring the concentrations of Sc_C³⁺ and Sc_A³⁺ in YSAG:Yb:Er solid solutions has been demonstrated.

Acknowledgements

This study was supported by the Russian Science Foundation Grant No. 23-23-00088, <https://rscf.ru/project/23-23-00088/>.

References

1. Yu Y., Wu Z., Zhang S. Concentration effects of Er³⁺ ion in YAG:Er laser crystals. *Journal of Alloys and Compounds*. 2000; 302(1-2): 204–208. [https://doi.org/10.1016/S0925-8388\(99\)00630-1](https://doi.org/10.1016/S0925-8388(99)00630-1)
2. Fei B., Chen W., Guo W., Shi M., Lin H., Huang Q., Zhang G., Cao Y. Optical properties and laser oscillation of Yb³⁺, Er³⁺ co-doped Y₃Al₅O₁₂ transparent ceramics. *Journal of Alloys and Compounds*. 2015; 636: 171–175. <https://doi.org/10.1016/j.jallcom.2015.01.203>
3. Basyrova L., Loiko P., Jing W., Wang Y., Huang H., Dunina E., Kornienko A., Fomicheva L., Viana B., Griebner U., Petrov V., Aguiló M., Díaz F., Mateos X., Camy P. Spectroscopy and efficient laser operation around 2.8 μm of Er:(Lu,Sc)₂O₃ sesquioxide ceramics. *Journal of Luminescence*. 2021; 240: 118373. <https://doi.org/10.1016/j.jlumin.2021.118373>
4. Mirhashemi A.H., Hossaini S.M.H., Etemadi A., Kharazifard M.J., Bahador A., Soudi A. Effect of Er:YAG and Er,Cr:YSGG lasers

- on ceramic bracket debonding from composite blocks. *Frontiers in Dentistry*. 2019; 16(2): 88–95. <https://doi.org/10.18502/fid.v16i2.1359>
5. Yassaie S., Aghili H., Firouzabadi A.H., Meshkani H. Effect of Er:YAG laser and sandblasting in recycling of ceramic brackets. *Journal of Lasers in Medical Sciences*. 2017; 8(1): 17–21. <https://doi.org/10.15171/jlms.2017.04>
 6. Quan J., Yang X., Long S., Yang M., Ma D., Huang J., Guo Y., Zhu Y., Wang B. Growth and fluorescence characteristics of Er:LuAG laser crystals. *Journal of Crystal Growth*. 2019; 507: 321–326. <https://doi.org/10.1016/j.jcrysgro.2018.11.037>
 7. Xu W., Hu Y., Jin Z., Zheng L., Zhang Z., Cao W. Anti-stokes excited Er³⁺/Yb³⁺ codoped oxyfluoride glass ceramic for luminescence thermometry. *Journal of Luminescence*. 2018; 203: 401–408. <https://doi.org/10.1016/j.jlumin.2018.06.081>
 8. Frej M.L., Valdez E., De Araújo C.B., Ledemi Y., Messaddeq Y. Stokes and anti-stokes luminescence of Er³⁺ doped Ga₁₀Ge₂₅S₆₅ glass excited at 980 and 532 nm. *Journal of Applied Physics*. 2010; 108(9): 093514. <https://doi.org/10.1063/1.3493239>
 9. Yang M., Sui Y., Mu H., Lü S., Wang X., Lü T. Mechanism of up-conversion emission enhancement in Y₃Al₅O₁₂:Er³⁺/Li⁺ powders. *Journal of Rare Earths*. 2011; 29(11): 1022–1025. [https://doi.org/10.1016/S1002-0721\(10\)60590-X](https://doi.org/10.1016/S1002-0721(10)60590-X)
 10. Shang Y., Chen T., Ma T., Hao S., Lv W., Jia D., Yang C. Advanced lanthanide doped upconversion nanomaterials for lasing emission. *Journal of Rare Earths*. 2022; 40(5): 687–695. <https://doi.org/10.1016/j.jre.2021.09.002>
 11. Kamińska I., Jankowski D., Sikora B., Kowalik P., Minikayev R., Wojciechowski T., Chojnacki M., Sobczak K., Rybusiński J., Szczytko J. Structural, optical and magnetic properties of Y_{3-0.02x}Er_{0.02}Yb_xAl₅O₁₂ (0 < x < 0.20) nanocrystals: effect of Yb content. *Nanotechnology*. 2020; 31(22): 225711. <https://doi.org/10.1088/1361-6528/ab73b9>
 12. Zhou J., Zhang W., Huang T., Wang L., Li J., Liu W., Jiang B., Pan Y., Guo J. Optical properties of Er,Yb co-doped YAG transparent ceramics. *Ceramics International*. 2011; 37(2): 513–519. <https://doi.org/10.1016/j.ceramint.2010.09.031>
 13. Tu L., Liu X., Wu F., Zhang H. Excitation energy migration dynamics in upconversion nanomaterials. *Chemical Society Reviews*. 2014; 44(6): 1331–1345. <https://doi.org/10.1039/c4cs00168k>
 14. Zheng B., Qi F., Yang J., Li B., Liu J., Zhang X., Wang P. Fabrication of Er:YAG/Yb:YAG nanopowder-derived Er:Yb co-doped silica fibers from UV-curable composites and their application in 1550-nm fiber lasers. In: Jáuregui-Misas C., Supradeepa V.R., eds. *Fiber Lasers XIX: Technology and Systems*. SPIE; 2022: 2. <https://doi.org/10.1117/12.2614271>
 15. Hlášek T., Rubešová K., Jakeš V., Jankovský O., Oswald J. Infrared luminescence in Er³⁺:Yb₃Al₅O₁₂ bulk ceramics prepared by sol-gel method. *Journal of the European Ceramic Society*. 2014; 34(15): 3779–3782. <https://doi.org/10.1016/j.jeurceramsoc.2014.06.017>
 16. Hlasek T., Rubešová K., Jakeš V., Nováček M., Oswald J., Fitl P., Siegel J., Macháč P. Physical vapor deposition of Er³⁺:Yb₃Al₅O₁₂ thin films from sol-gel derived targets. *Ceramics-Silikáty*. 2016; 60(4): 285–290. <https://doi.org/10.13168/cs.2016.0043>
 17. Zhang P., Chen Z., Hang Y., Li Z., Yin H., Zhu S., Fu S., Li A. Enhanced emission of the 1.50–1.67 μm fluorescence in Er³⁺, Ce³⁺-codoped Lu₃Al₅O₁₂ crystal. *Journal of Alloys and Compounds*. 2017; 696: 795–798. <https://doi.org/10.1016/j.jallcom.2016.12.003>
 18. You Z., Wang Y., Xu J., Zhu Z., Li J., Wang H., Tu C. Single-longitudinal-mode Er: GGG microchip laser operating at 2.7 μm. *Optics Letters*. 2015; 40(16): 3846–3849. <https://doi.org/10.1364/OL.40.003846>
 19. Dong J., Ueda K.-I., Kaminskii A.A. Optical properties and laser operation of Yb:Y₃Sc₂Al₃O₁₂ crystal. In: *Conference on Lasers and Electro-Optics/Pacific Rim 2009*; 2009: 2. <https://doi.org/10.1109/CLEOPR.2009.5292564>
 20. Dong J., Ueda K.-I., Kaminskii A.A. Continuous-wave and Q-switched microchip laser performance of Yb:Y₃Sc₂Al₃O₁₂ crystals. *Optics Express*. 2008; 16(8): 2565–2573. <https://doi.org/10.1364/OE.16.005241>
 21. Ma J., Wang J., Shen D., Ikesue A., Tang D. Generation of sub-100-fs pulses from a diode-pumped Yb:Y₃ScAl₄O₁₂ ceramic laser. *Chinese Optics Letters*. 2017; 15(12): 121403. <https://doi.org/10.3788/COL201715.121403>
 22. Tarala V.A., Nikova M.S., Kuznetsov S.V., Chikulina I., Kravtsov A.I., Vakalov D., Krandievsky S.O., Malyavin F.F., Ambarsumov M., Kozhitov L.V., Mitrofanenko L.M. Synthesis of Y₃Al₅O₁₂:Er ceramics and the study of the scandium impact in the dodecahedral and octahedral garnet sites on the Er³⁺ energy structure. *Journal of Luminescence*. 2022; 241: 118539–118543. <https://doi.org/10.1016/j.jlumin.2021.118539>
 23. Xia Z., Meijerink A. Ce³⁺-doped garnet phosphors: Composition modification, luminescence properties and applications. *Chemical Society Reviews*. 2017; 46(1): 275–299. <https://doi.org/10.1039/c6cs00551a>
 24. Tarala V.A., Kuznetsov S.V., Chapura O.M., Malyavin F.F., Brazhko E.A., Kravtsov A.A. Fabrication and optical properties of garnet ceramics based on Y_{3-x}Sc_xAl₅O₁₂ doped with ytterbium and erbium. *Dalton Transactions*. 2023, 52(32): 11285–11296. <https://doi.org/10.1039/D3DT01453C>
 25. Tarala V.A., Shama M.S., Chikulina I.S., Kuznetsov S.V., Malyavin F.F., Vakalov D.S., Kravtsov A.A., Pankov M.A. Estimation of Sc³⁺ solubility in dodecahedral and octahedral sites in Y₃Al₅O₁₂:Yb. *Journal of the American Ceramic Society*. 2019; 102(8): 4862–4873. <https://doi.org/10.1111/jace.16294>
 26. Nikova M.S., Tarala V.A., Malyavin F.F., Chikulina I.S., Vakalov D.S., Kravtsov A.A., Krandievsky S.O., Lapin V.A., Medyanik E.V., Kozhitov L.V., Kuznetsov S.V. Sintering and microstructure evolution of Er_{1.5}Y_{1.5-x}Sc_{x+y}Al_{5-y}O₁₂ garnet ceramics with scandium in dodecahedral and octahedral sites. *Journal of the European Ceramic Society*. 2022; 42(5): 2464–2477. <https://doi.org/10.1016/j.jeurceramsoc.2022.01.008>
 27. Database of Ionic Radii. <http://abulafia.mt.ic.ac.uk/shannon/ptable.php>
 28. Denton A.R., Ashcroft N.W. Vegard's law. *Physical Review A*. 1991; 43(6): 3161–3164. <https://doi.org/10.1103/PhysRevA.43.3161>

29. Stročka B., Holst P., Tolksdorf W. An empirical formula for the calculation of lattice constants of oxide garnets based on substituted yttrium- and gadolinium-iron garnets. *Philips Journal of Research*. 1978; 33: 186–202.
30. Vorobiov Y.P., Carban O.V. A new empirical formula for the calculation of an elementary cell parameter of synthetic oxides-garnets. *Journal of Solid State Chemistry*. 1997; 134(2): 338–343. <https://doi.org/10.1006/jssc.1997.7570>
31. Erhart P. A first-principles study of helium storage in oxides and at oxide-iron interfaces. *Journal of Applied Physics*. 2012; 111(11): 113502. <https://doi.org/10.1063/1.4707944>
32. Nikova M., Tarala V.A., Malyavin F.F., Vakalov D.S., Lapin V.A., Kuleshov D.S., Kravtsov A.A., Chikulina I.S., Tarala L.V., Evtushenko E.A., Medyanik E.V., Krandievsky S.O., Bogach A.V., Kuznetsov S.V. The scandium impact on the sintering of YSAG:Yb ceramics with high optical transmittance. *Ceramics International*. 2021; 47(2): 1772–1784. <https://doi.org/10.1016/j.ceramint.2020.09.003>
33. Hrabovský J., Kucera M., Paloušová L., Bi L., Veis M. Optical characterization of Y₃Al₅O₁₂ and Lu₃Al₅O₁₂ single crystals. *Optical Materials Express*. 2021; 11(4): 1218–1223. <https://doi.org/10.1364/OME.417670>
34. Allik T.H., Morrison C.A., Gruber J.B., Kokta M.R. Crystallography, spectroscopic analysis, and lasing properties of Nd³⁺:Y₃Sc₂Al₃O₁₂. *Physical Review B*. 1990; 41(1): 21–30. <https://doi.org/10.1103/PhysRevB.41.21>
35. Kuwano Y., Suda K., Ishizawa N., Yamada T. Crystal growth and properties of (Lu, Y)₃Al₅O₁₂. *Journal of Crystal Growth*. 2004; 260: 159–165. <https://doi.org/10.1016/j.jcrysgro.2003.08.060>
36. Pujol M.C., Maitre A., Carreaud J., Boulesteix R., Brenier A., Alombert-Goget G., Guyot Y., Carvajal J.J., Solé R.M., Massons J., Oleaga A., Salazar A., Gallardo I., Moreno P., Vázquez de Aldana J.R., Aguiló M., Diaz F. Thermal and Optical Characterization of Undoped and Neodymium-Doped Y₃ScAl₄O₁₂ Ceramics. *The Journal of Physical Chemistry C*. 2014; 118(25): 13781–13789. <https://doi.org/10.1021/jp5027493>
37. Tarala V.A., Suprunchuk V.E., Kravtsov A.A., Malyavin F.F., Vakalov D.S., Tarala L.V., Lapin V.A., Chapura O.M., Medyanik E.V., Dziof D.T., Kuznetsov S.V. Fabrication and Optical Properties of YSAG:Cr Optical Ceramics. *Ceramics International*. 2023; 49(19): 32127–32135. <https://doi.org/10.1016/j.ceramint.2023.07.181>
38. Tang F., Wang W, Yuan X., Zhu C., Huang J., Ma C., Wang F., Lin Y., Cao Y. Dependence of optical and thermal properties on concentration and temperature for Yb:YAG laser ceramics. *Journal of Alloys and Compounds*. 2014; 593: 123–127. <https://doi.org/10.1016/j.jallcom.2013.12.194>
39. Dong J., Bass M., Mao Y., Deng P., Gan F. Dependence of the Yb³⁺ emission cross section and lifetime on temperature and concentration in yttrium aluminum garnet. *Journal of the European Ceramic Society*. 2003; 20(9): 1975–1979. <https://doi.org/10.1364/JOSAB.20.001975>
40. Gruber J.B., Quagliano J.R., Reid M.F., Richardson F.S., Hills M.E., Seltzer M.D., Stevens S.B., Morrison C.A., Allik T.H. Energy levels and correlation crystal-field effects in Er³⁺-doped garnets. *Physical Review B*. 1993; 48(21): 15561–15573. <https://doi.org/10.1103/PhysRevB.48.15561>
41. Liu M., Wang S., Zhang J., An L., Chen L. Preparation and up-conversion luminescence of Y₃Al₅O₁₂:Yb³⁺, Er³⁺ transparent ceramics. *Journal of Rare Earths*. 2006; 24(6): 732–735. [https://doi.org/10.1016/S1002-0721\(07\)60018-0](https://doi.org/10.1016/S1002-0721(07)60018-0)
42. Liu M., Wang S.W., Zhang J., An L.Q., Chen L.D. Dominant red emission (⁴F_{9/2} → ⁴I_{15/2}) via upconversion in YAG (Y₃Al₅O₁₂):Yb³⁺,Er³⁺ nanopowders. *Optical Materials*. 2007; 29(11): 1352–1357. <https://doi.org/10.1016/j.optmat.2006.03.028>
43. Desirena H., Diaz-Torres L.A., Rodríguez R.A., Meza O., Salas P., Angeles-Chávez C., Tobar E.H., Castañeda-Contreras J., De la Rosa E. Photoluminescence characterization of porous YAG:Yb³⁺–Er³⁺ nanoparticles. *Journal of Luminescence*. 2014; 153: 21–28. <https://doi.org/10.1016/j.jlumin.2014.03.012>
44. Xu H., Zhou L., Dai Z., Jiang Z. Decay properties of Er³⁺ ions in Er³⁺:YAG and Er³⁺:YAlO₃. *Physica B: Condensed Matter*. 2002; 324(1-4): 43–48. [https://doi.org/10.1016/S0921-4526\(02\)01231-0](https://doi.org/10.1016/S0921-4526(02)01231-0)